Published in final edited form as:
J Am Chem Soc. 2009 July 29; 131(29): 10211–10219. doi:10.1021/ja902557r.

A Combined Theoretical and Experimental Study of the Ammonia Tunnel in Carbamoyl Phosphate Synthetase

Yubo Fan, **Liliya Lund**, **Qiang Shao**, **Yi-Qin Gao***, and **Frank M. Raushel***
Department of Chemistry, Texas A&M University, College Station, Texas 77843

Abstract

The transfer of ammonia in carbamoyl phosphate synthetase (CPS) was investigated by molecular dynamics simulations and experimental characterization of mutations within the ammonia tunnel. In CPS, ammonia is derived from the hydrolysis of glutamine and this intermediate must travel ~45 Å from the site of formation in the small subunit to the site of utilization in the large subunit. In this investigation the migration of ammonia was analyzed from the exit of the small subunit through the large subunit where it ultimately reacts with the carboxy phosphate intermediate. Potential of mean force calculations along the transfer pathway for ammonia indicate a relatively low free energy barrier for the translocation of ammonia. The highest barrier of 7.2 kcal/mol is found at a narrow *turning gate* surrounded by the side chains of Cys-232, Ala-251 and Ala-314 in the large subunit. The environment of the ammonia tunnel from the exit of the small subunit to the turning gate in the tunnel is filled with clusters of water molecules and the ammonia is able to travel through this area easily. After ammonia passes through the turning gate it enters a hydrophobic passage. A hydrogen bond then forms between the ammonia and Thr-249, which facilitates the delivery to a more hydrophilic environment near the active site for the reaction with the carboxy phosphate intermediate. The transport process from the turning gate to the end of the tunnel is favored by an overall down-hill free energy potential and no free energy barrier higher than 3 kcal/mol. A conformational change of the turning gate, caused by formation of the carboxy phosphate intermediate, is consistent with a mechanism in which the reaction between ATP and bicarbonate triggers the transport of ammonia and consequently accelerates the rate of glutamine hydrolysis in the small subunit. A blockage in the turning gate passageway was introduced by the triple mutant C232V/A251V/A314V. This mutant is unable to synthesize carbamoyl phosphate using glutamine as a nitrogen source.

INTRODUCTION

Carbamoyl phosphate synthetase (CPS) from *Escherichia coli* catalyzes one of the most complex reactions in biological chemistry. The product of this enzymatic transformation, carbamoyl phosphate, is utilized in the biosynthesis of arginine and pyrimidine nucleotides.[1-3] Carbamoyl phosphate is formed from glutamine, bicarbonate and two molecules of MgATP through a series of four separate reactions.[4] The generally accepted reaction mechanism is summarized in Scheme 1. In the initial reaction, the first molecule of ATP is used to phosphorylate bicarbonate to generate the reactive intermediate, carboxy phosphate. Glutamine is hydrolyzed to glutamate and ammonia, followed by the reaction of ammonia with

*To whom correspondence may be sent: (YQG) telephone: (979) 458−0592, fax: (979) 845−4719; e-mail; yiqin@mail.chem.tamu.edu (FMR) telephone: (979) 845−3373; fax: (979) 845−9452; e-mail: raushel@tamu.edu.

SUPPORTING INFORMATION **AVAILABLE**. The computational details and the complete authors for references 41 and 42 are provided in addition to the CD spectra for the mutant enzymes. A short movie that shows the movement of ammonia from the site of formation in the small subunit to the site of utilization in the large subunit is available. This material is available free of charge via the Internet at http://pubs.acs.org.

the carboxy phosphate intermediate to form carbamate. Finally, a second molecule of ATP is used to phosphorylate carbamate to form the ultimate product, carbamoyl phosphate. There are thus four separate reactions and three discrete, reactive, and unstable intermediates involved in this reaction mechanism: carboxy phosphate, ammonia, and carbamate.[5,6]

The protein isolated from *E. coli* is a heterodimer composed of a small (42 kDa) and a large (118 kDa) subunit. Structural data has confirmed the presence of three spatially distinct active sites that are linked by two long molecular tunnels that extend approximately 100 Å from one end of the protein to the other (Figure 1). The small subunit contains the active site for the hydrolysis of glutamine, which is hydrolyzed to glutamate and ammonia via a thioester intermediate.[7-9] The ammonia derived from this reaction travels ~45 Å to the active site for the synthesis of the carboxy phosphate intermediate, located in the N-terminal half of the large subunit. The carbamate intermediate, formed by the reaction of ammonia with carboxy phosphate, is subsequently channeled ~45 Å to the active site for the synthesis of carbamoyl phosphate. This active site is located within the C-terminal half of the large subunit where carbamate is phosphorylated by the second molecule of MgATP to form the ultimate product, carbamoyl phosphate[3, 10]. CPS thus contains two long molecular tunnels for the transport of ammonia and carbamate.

Intramolecular protein tunnels have been found in a number of enzymes where it is necessary to shelter unstable and reactive intermediates from bulk solution. Tunnels for the translocation of ammonia have been found in all members of the amidotransferase family for which structural data is available.[11-20] All of these enzymes utilize ammonia derived from the hydrolysis of glutamine.[21,22] Isotopic labeling studies have demonstrated that the ammonia derived from the hydrolysis of glutamine in CPS does not exchange with added ammonia present in the bulk solution.[23] These data demonstrate that the wild type enzyme is not leaky and that there is a strong coupling between the reactions at the separate active sites. Unfortunately, there are significant difficulties in experimentally tracking the migration of ammonia from one active site to the next.

Molecular dynamics (MD) simulations can serve as a useful tool to investigate the kinetic and dynamic details of the mechanism for ammonia migration at the atomic level. For example, the transfer of NH_3 in imidazole glycerol phosphate synthase and glucosamine-6-phosphate synthase has been studied using steered MD.[25-27] The free energy profile for NH_3 transport in AmtB was calculated by an umbrella sampling technique and it was also investigated at an elevated temperature of 323 K utilizing conventional MD simulations.[28-24] These simulations have led to a better understanding of the transport mechanisms for ammonia and helped to explain the conformational changes of key residues in these proteins.

We have previously examined the mechanism for the migration of ammonia by MD simulations from the site of synthesis in the small subunit to the interface between the small and large subunits.[25] The simulations revealed a two-step mechanism in which ammonia is solvated into a water pocket containing 5−7 waters by overcoming a low barrier of 3.7 kcal/mol. A stabilization of more than 7 kcal/mol in free energy is gained in the first step and then the ammonia travels through a relatively narrow passage leading to the exit of the small subunit by overcoming a barrier of 5.7 kcal/mol in the second step. These conclusions were supported by multiple trajectories for ammonia transport over a distance of ~13 Å without introducing any biasing forces.

In this paper, we calculate the free energy profile for the remainder of the ammonia tunnel within CPS using the umbrella sampling technique. From these studies and earlier studies it is found that the transport of ammonia through the entire tunnel is composed roughly of three steps. First, the ammonia is injected into the tunnel with a free energy drop of more than 7 kcal/

mol and this is followed by an energy-flat region between His-353 and Ser-35 in the small subunit.[25] Second, after passing through the relatively narrow portion of the tunnel near Ser-35 and Thr-37 in the small subunit, the ammonia enters the large subunit. In this region, two large water clusters are separated by Tyr-261 and the ammonia moves back and forth fairly freely between these two clusters. Finally, after overcoming a narrow turning gate surrounded by the side chains from Cys-232, Ala-251 and Ala-314 in the large subunit the ammonia passes through a hydrophobic corridor with the help of a strong hydrogen bond to Thr-249. The ammonia then travels through a free energy-downhill region without any barrier higher than 3 kcal/mol to the site of synthesis for carboxy phosphate and carbamate.

MATERIALS and METHODS

Construction of Models for the Thioester Intermediate

The X-ray crystal structure of CPS (PDB code: 1cs0) was taken as the starting point for the simulations of NH_3 transfer in this enzyme.[26] The residues Met-1, Ala-381 and Lys-382 from the small subunit of CPS are missing in this X-ray structure and they were added manually with extended conformations during the simulations. The two missing loops, 717−723 and 742−749, in the large subunit of CPS were inserted using SWISS-MODEL.[27-29] These two loops are part of the binding site for ATP in the carbamoyl phosphate synthesis domain. This binding site is ~45 Å away from the other ATP binding site that is utilized for the synthesis of carboxy phosphate and carbamate. In this structure the wild type CPS is bound with a glutamate γ-semialdehyde inhibitor in the active site of the small subunit. The thiol group of Cys-269 forms a covalent bond with the side chain aldehyde group to generate a tetrahedral addition complex that mimics the proposed tetrahedral intermediate for amide bond hydrolysis. In the simulations reported here, the inhibitor covalently bonded with Cys-269 was replaced with a γ-glutamyl cysteine residue (Cyg). The geometry of the Cyg group was optimized to a local minimum and the conformation of the side chain was kept the same as the substituted Cys-269 of the wild type enzyme.

The charge distributions on all atoms in Cyg and NH_3 were obtained using the RESP-fit method[30,31] based on B3LYP/cc-pVTZ calculations[32-35] with the solvent effect ($\varepsilon = 4$) taken into account using the polarizable continuum model (PCM).[36-38] The geometry for NH_3 was fully optimized in the gas phase at the same level as that for the charge distribution calculations. The charge on the nitrogen atom in NH_3 was −0.9882. All of the crystalline waters within the enzyme or on the protein exterior, including Mn^{2+}, K^+ and Cl−, were utilized for the simulations. It is important to point out that K^+ and Cl− move freely during these simulations while Mn^{2+} ions are tightly bound to ADP and/or phosphate. The protonation states of all histidine residues were adjusted based on the local environments. For example, N_δ of His-353 from the small subunit is protonated because this nitrogen atom is within H-bonding distance of the side chain carboxylate of Glu-355. The net negative charge in the protein was neutralized by added Na^+ ions. Explicit TIP3P waters were added as a truncated octahedral water box with an 8 Å buffer.[39] All operations were processed using the AMBER Leap module, which led to models containing ~120,000 atoms, including ~39,000 waters. [40,41] These models were further extended using the periodic boundary condition. The AMBER force field 99,[42] with the parameters for the peptide backbone reoptimized, was utilized for all standard amino acid residues and NH_3, while the general AMBER force field was used for the sulfur-related bonds, bond angles and torsional angles in the γ-glutamyl thioester intermediate.[43] The force field for ADP[44], P_i[44] and Mn^{2+} [45] are contributed by Richard Bryce at the University of Manchester. MD simulations were conducted in the isothermal–isobaric (NPT) ensemble at 300 K and 1 atm. The SHAKE algorithm was used to constrain all bonds involving hydrogens.[46] A 10.0 Å cutoff was applied for nonbonding interactions. The Particle Mesh Ewald method was employed to treat the long-range electrostatic interactions.[47,48]

MD trajectories were obtained on these structures using the AMBER suite of programs.[40,41] Before the MD simulations, in which the trajectories were collected every 0.5 ps, two steps of minimization were conducted. During minimization, the systems were first optimized for 1000 cycles while the backbone of the protein was frozen with a force constant of 500.0 kcal/mol/Å^2. The systems were further optimized for 2500 cycles without constraints, followed by a 20-ps MD simulation which heats the system from 0 K to 300 K, with a force constant of 10.0 kcal/mol/Å^2 added upon the protein backbone. A 200-ps simulation under 1 atm and 300 K was performed to reach equilibrium with the constraints on the protein removed . All data were collected from the MD simulations.

Free Energy Calculations

For the convenience of choosing an appropriate reaction coordinate, the ammonia tunnel in the large subunit of CPS was separated into two approximately linear sections during the free energy calculations. As shown in Figure 2, the reaction coordinate in the first part (shown by the red arrow) of the free energy calculations is defined as the distance between the nitrogen atom of the ammonia and the carbonyl carbon of the thioester intermediate in Cyg-269. In the second part, the reaction coordinate is defined as the distance between the ammonia nitrogen and one of the Mn^{2+} ions in the active site for the formation of carbamate (shown by the blue arrow). The first half of the ammonia tunnel in the large subunit extents from the exit of the ammonia tunnel near residues Ser-35 and Thr-37 of the small subunit to a turning gate, constricted by the side chains of Cys-232, Ala-251 and Ala-314 from the large subunit. The second portion of the tunnel extends from this constriction to the end of the ammonia tunnel. The free energy profiles or potentials of mean force (PMF) along the tunnel were computed using the umbrella sampling technique with a biasing harmonic potential involving a force constant of 40 kcal/mol/Å^2.[49-53] The PMF for the first segment was calculated using 104 windows chosen from the trajectories with NH_3 positioned at discrete sites of the tunnel while that for the second portion of the tunnel was sampled using 45 windows. For each window, a 10-ps equilibration simulation was performed and a subsequent 400-ps simulation was used to generate dynamics data for the WHAM (Weighted Histogram Analysis Method) analyses.[50-52]

Bacterial Strains and Plasmids

Site-directed mutagenesis of CPS was performed as described previously.[54,55] The RC50 strain used for protein expression was a generous gift from Dr. Carol J. Lusty. All plasmids used in this project were derived from pMS03.[54] Oligonucleotide synthesis and DNA sequencing reactions were performed by the Gene Technology Laboratory, Texas A&M University.

Construction and Purification of Mutant Proteins

Site-directed mutagenesis was performed using the Quick Change protocol from Stratagene. All of the site-directed changes made to the wild-type CPS were confirmed by DNA sequencing of the modified plasmids. The plasmids containing the *car*AB genes were transformed in the RC50 cell line of *E. coli* for expression of the wild-type and mutant forms of CPS. The wild-type and mutant variants of CPS were purified as previously described.[56] The mutants S35Y, C232V/A251V/A314V, C232G/A251G/A314G, A251C, A314C, A311L, I352F and T249V in the ammonia tunnel were expressed and purified to greater than 95% homogeneity, as judged by SDS-polyacrylamide gel electrophoresis.

Circular Dichroism Measurements

The secondary structure of all mutant proteins was determined using circular dichroism measurements. All measurements were made on an Aviv 62DS spectropolarimeter. Each

sample contained 450 nM protein in 5 mM phosphate buffer, pH 7.6. Measurements were made using quartz cuvettes with a 1-cm path length.

Kinetic Measurements

The rate of glutamine hydrolysis was determined by coupling the formation of glutamate to the production of α-ketoglutarate with L-glutamate dehydrogenase and 3-acetylpyridine adenine dinucleotide (APAD).[54] The reaction mixtures contained 50 mM Hepes (pH 7.6), 20 mM $MgCl_2$, 100 mM KCl, 40 mM $KHCO_3$, 5.0 mM ATP, 10 mM ornithine, 1.0 mM APAD, 30 U L-glutamate dehydrogenase, and varying amounts of glutamine. The rate of ADP formation was measured using a pyruvate kinase/lactate dehydrogenase coupling system.[56] The reaction mixtures for the glutamine-dependent assay contained 50 mM Hepes, pH 7.6, 20 mM $MgCl_2$, 100 mM KCl, 40 mM $KHCO_3$, 10 mM glutamine, 10 mM ornithine, 1.0 mM phosphoenolpyruvate, 0.2 mM NADH, 2 units of pyruvate kinase, 3 units of lactate dehydrogenase, and varying amounts of ATP. Glutamine was excluded from the bicarbonate-dependent and NH_4^+-dependent ATPase assays. Varying amounts of NH_4Cl and 5 mM ATP were used for the NH_4^+-dependent ATPase assay. Both of these assays were followed by the decrease in absorbance at 340 nm using a Molecular Devices SpectraMax Plus 96-well plate reader. The synthesis of carbamoyl phosphate was determined by measuring the rate of citrulline formation in a coupled assay containing ornithine transcarbamoylase (OTCase) and ornithine.[57] The assay mixture contained 50 mM Hepes, pH 7.6, 20 mM $MgCl_2$, 100 mM KCl, 40 mM $KHCO_3$, 5.0 mM ATP, 10 mM ornithine, 12 units of OTCase, and 10 mM glutamine. The rate of ATP synthesis was measured with a hexokinase/glucose-6-phosphate dehydrogenase (G6PDH) coupling system.[54] The assay mixture for the ADP-dependent assay included 50 mM Hepes, pH 7.6, 20 mM $MgCl_2$, 100 mM KCl, 10 mM ornithine, 0.75 mM NAD, 2 units of hexokinase, 1.0 mM glucose, 1 unit of G6PDH, 1.0 mM carbamoyl phosphate, and varying amounts of ADP.

RESULTS and DISCUSSION

Translocation of NH_3 into the Large Subunit

Ammonia is generated as a reactive intermediate in CPS as a result of glutamine hydrolysis in an active site located in the small subunit. The MD simulations for the passage of ammonia through the small subunit of CPS have been described previously.[25] In these studies it was found that as the ammonia approaches the interface between the large and small subunits of CPS it is largely desolvated from a water cluster and passes by Ser-35 and Thr-37.[25] The PMF along the ammonia tunnel from the exit of the small subunit near residue Thr-37 to a narrow turning point in the tunnel that is gated by a constriction formed by the side chains of Cys-232, Ala-251 and Ala-314 is shown in Figure 3. This portion of the free energy profile is roughly characterized by two maxima. The first peak is located near Tyr-261 at a distance of approximately 22 Å from Cys-269. The second maximum occurs at a distance of approximately 30 Å where the tunnel makes a sharp bend at a turning point that leads to the next active site at the end of the ammonia tunnel. The barrier here is 7.2 kcal/mol. Between Thr-37 in the small subunit and Tyr-261 in the large subunit the relative free energy for the translocation of ammonia is generally flat. The lowest free energy well occurs in a region after Tyr-261 at a distance of approximately 24 Å. The side chain of Tyr-261 extends into this water reservoir and partitions it into two pockets of water. These two water clusters can exchange water fairly freely with each other because of the flexibility of the Tyr-261 side chain, which does not form a hydrogen bond to any other residues and thus is able to interact strongly with the waters in either cluster.

The first water pocket is well-formed by the surrounding residues as shown in the connected surface model in Figures 4a and b. This segment of the ammonia tunnel corresponds to the

fairly flat region of the PMF plot presented in Figure 3 at a distance of 15 to 21 Å from the thioester intermediate in the small subunit. Thr-37 from the small subunit and Tyr-261 from the large subunit narrow the tunnel and as a result the water cluster is effectively dissected into two parts. A 16-ns trajectory of conventional MD simulation, started with the ammonia positioned in the first water pocket, reveals the stability for ammonia solvation in the water cluster and the flexibility of Tyr-261, as illustrated in Figure 5a. Based on the calculated distribution function of the distance between the ammonia and the hydroxyl oxygen of Thr-37, the ammonia is completely solvated in the water cluster (the major peak at ~6 Å of curve II in Figure 5a) while Thr-37 can still form a hydrogen bond with ammonia (the small peak at about 2.8 Å). Solvation in the next water pocket is responsible for the relatively low but even distribution at 7 to 10 Å (curve II in Figure 5a)

The second water pocket is located between Tyr-261 and the turning point gated formed by Cys-232, Ala-251 and Ala-314 as illustrated in Figures 4c and 4d. This pocket is enclosed by the residues forming the tunnel wall and is only open to Tyr-261 and the gate. The side chain of Tyr-354 is constrained due to a hydrogen bond to the carbonyl oxygen of Ala-314 in the protein backbone. Because this spacious pocket is capable of accommodating a large water cluster, ammonia can be efficiently solvated in this pocket. Consequently a deep free energy well is observed at about 24 Å in Figure 3. The free energy profile is much simpler for the second water pocket because it lacks nearby hydrophilic residues except for Ser-233. The intermolecular interactions in the first water pocket is made complex as a result of the exchange of hydrogen bonds between ammonia and the hydrophilic residues, Tyr-255 and Tyr-257 from the large subunit, and Thr-37 in the small subunit. Based on the distance distribution between the ammonia and C_β of Cys-232, calculated from a 5-ns trajectory of conventional MD simulation that started with ammonia placed between Cys-232 and Tyr-261, a single large peak at about 5 Å (see curve I in Figure 5b) is identified. This confirms that ammonia is adequately solvated and significantly stabilized in this water pocket. Furthermore, the low probability distribution in the range from 9 to 18 Å indicates that Tyr-261 only partly ruptures the connection between this pocket and the first one, again indicating that the free energy barrier separating these two pockets is not very high. The barriers for the forward and reverse ammonia transport are about 1.9 and 3.9 kcal/mol in free energy, respectively. In addition, the excellent solvation of ammonia in the pocket between Tyr-261 and the gate is confirmed by the major peak at about 10 Å of curve II in Figure 5b while a hydrogen bond between the ammonia and the side chain hydroxyl of Thr-37 from the small subunit was observed (see the small peak at about 2.8 Å).

To move further along the tunnel, the ammonia has to overcome a barrier of 7.2 kcal/mol at a gate composed of Cys-232, Ala-251 and Ala-314. This transition corresponds to the peak at ~30 Å in Figure 3. The dimension of the gate is barely enough for a single ammonia to pass because the radius for the largest contact sphere in this triangle of residues ranges from 0.3 to 2.9 Å (based on the triangle shown in Figure 6 and the van der Waals radii for the atoms involved in the triangle.). This width is very close to the van der Waals radius of 1.824 Å for ammonia. Apparently, the requirement for dehydration of ammonia impedes the passage through the gate and none of the three surrounding residues is able to form a hydrogen bond to compensate for the loss of water solvation. The tunnel makes a turn of about 90° after the gate (see Figure 2).

Translocation of NH_3 from the Turning Gate to the Site of Carbamate Formation

After overcoming the barrier at the turning gate formed by the intersection of Cys-232, Ala-251 and Ala-314, the free energy profile for the ammonia transport has an overall downhill trend. This is illustrated in Figure 7a. The ammonia reaches the end of the tunnel and the global free energy minimum at about 8 Å from the bound Mn^{2+}, where the ammonia interacts with the

phosphate (during catalysis carboxy phosphate would react with the ammonia) and Arg-306 by forming hydrogen bonds. The passage leading to the active site is confined by an α-helix and a β-strand as shown in Figure 7b. The local minimum between 15 to 18 Å in Figure 7a corresponds to the space between the gate triad and another triad formed from the side chains of Ile-234, Thr-249 and Leu-310. In the MD trajectories, neither water nor amino acid residues form hydrogen bonds to the ammonia except for the side chain hydroxyl of Thr-249, which remains intact until the ammonia is delivered to the site for the binding of ATP. Even more striking, no water is located in any trajectory computed using conventional MD even when the ammonia is not in this region. Apparently, ammonia must be completely desolvated when it is transported through this extremely hydrophobic passage, the length of which (from Cys-232 to Thr-249) is at least 9 Å.

Due to the loss of stabilization by solvation, it is not favorable for ammonia to move through the turning gate. The free energy profile in this region is higher than that before ammonia passes the gate by about 3 kcal/mol (see the free energy at 24 and 32 Å in Figure 3). Desolvation consumes more than 6 kcal/mol when the ammonia passes through the gate but the hydrogen bond to Thr-249 contributes about 3 kcal/mol after the passing. The barrier of ~3.6 kcal/mol, located at 14.6 Å, corresponds to the narrow passage surrounded by Ile-234, Thr-249 and Leu-310. When ammonia passes through this region, there are strong steric effects from Ile-234 and Leu-310 due to the rigidity of the hydrogen bond between the ammonia and Thr-249. The ammonia is subsequently delivered from the side chain of Thr-249 to the next hydrophilic area filled with at least 26 waters. These water molecules are in the region between Thr-249 and the bound phosphate, and are surrounded by Glu-217, Thr-244, Thr-249, Arg-206 and Ser-307. This water cluster directly extends and connects to the exceptionally hydrophilic binding site for ATP (ADP and P_i in the simulation), which is surrounded by water. The hydrogen bond between the ammonia and the hydroxyl from the side chain of Thr-249 is formed after the ammonia passes the turning gate and persists until the ammonia is sufficiently solvated by the water cluster in the next hydrophilic region. This hydrogen bond is kept in the reaction coordinate range of 18−12 Å as shown in Figure 7a.

A barrier of about 3 kcal/mol in free energy is located in the area surrounded by Glu-217, Thr-244 and Ser-307 when the ammonia approaches the active site for carbamate formation. This barrier is responsible for breaking of the strong hydrogen bond network formed by Glu-217, Arg-306 and Ser-307, especially the salt bridge between Glu-217 and Arg-306 when the ammonia moves towards the phosphate.

Influence of Carboxy Phosphate Formation on the Turning Gate

Ala-314 of the turning gate and Arg-306, which binds the phosphate in the X-ray crystal (or the γ-phosphoryl group of ATP) are located at opposite ends of the same α-helix. Therefore, changing the ligands to Arg-306 upon carboxy phosphate formation is expected to alter the protein conformation near the gate. Thus, the opening and closing of the turning gate at Ala-314 could be controlled by the reaction occurring at the site that is mediated by Arg-306. To test this possibility, two separate umbrella sampling simulations were performed for P_i-bound and carboxy phosphate-bound CPS and the free energy profiles are shown in Figure 8. For both calculations the distance from the ammonia to Ser-307 on the α-helix was defined as the reaction coordinate (see Figures 8b and 8c) and the PMFs were calculated using 46 windows. In the case of carboxy phosphate, the phosphate moiety occupies the same position as P_i while the carboxylate moiety binds between the phosphate and Arg-306 and interacts with the arginine by forming hydrogen bonds. As shown in Figure 8a, the barrier near the turning gate with carboxy phosphate-bound is about 1.8 kcal/mol lower than that with P_i-bound (see the barriers at 6.3 Å and 7.5 Å for the blue and red curves, respectively). Moreover, compared to the case with P_i-bound, the stable water pocket shown in Figure 4b is about 1 Å closer to

Ser-307 in the carboxy phosphate-bound structure. That is to say, the carboxy phosphate pushes the α-helix and the subsequent movement of Ala-314 expands the gate and thus makes it easier for ammonia to enter. As shown in Figure 8c, the carboxyl group in the carboxy phosphate interacts directly with Arg-306 while the phosphate group is still bound in the original position (see Figure 8b). The strong ion-ion and hydrogen bond interactions push the α-helix (residues 306 to 315 in the large subunit) and as a result the gate circled by Cys-232, Ala-251 and Ala-314 is expanded. These results are qualitatively in agreement with the experimental observation that the hydrolysis of glutamine is 30-fold faster in the presence of bicarbonate and ATP compared to that in the absence of these substrates.

Rate Limiting Step for Ammonia Transfer

The narrow gate, which is created by the conjunction of Cys-232, Ala-251 and Ala-314, results in a barrier of 7.2 kcal/mol. In this study, we used Kramers' reaction rate theory in solution (Equation 1), assuming that the dynamics can be described by a one-dimensional diffusion along a reaction coordinate in which both the reactant well and the barrier top are parabolic, to estimate the rates in complex environments.[58-60] In Equation 1, $\omega_{\min}$ and $\omega_{\max}$ are frequencies that characterize the curvature of the free energy profile at the minimum and the barrier top, respectively; k_B is Boltzmann's constant, T is the absolute temperature; h is Planck's constant; ΔG^* is the height of the free energy barrier and R is universal gas constant; and $D_{\min}$ and $D_{\max}$ are the diffusion constants at the minimum and the barrier top, respectively, shown in Figure 3. $D_{\min}$ for ammonia and $\omega_{\min}$ were fit to 0.00418 $Å^2$/ps and 1.013 s^{-1}, respectively. Thus, from Equation 1, τ = 101 μs, which means that it takes ammonia ~100 μs to traverse the free energy barrier imposed by the narrow gate surrounded by Cys-232, Ala-251 and Ala-314 shown in Figure 3. The diffusion through the rest of the tunnel is fast and the estimated rate constant for this step is 9.9 ms^{-1}, which is ~200-fold faster than the rate constant for the overall synthesis of carbamoyl phosphate. Therefore, the overall barrier for the transport of ammonia through the protein interior is too low to be the rate-determining step for this enzyme.

$$\tau = \frac{2\pi k_B T}{\omega_{\min}\omega_{\max}D_{\max}}\exp\left(\frac{\Delta G^*}{RT}\right) \approx \frac{2\pi k_B T}{\omega_{\min}^2 D_{\min}}\exp\left(\frac{\Delta G^*}{RT}\right) \quad (1)$$

Mutation of Tunnel Residues

Amino acid residues within the ammonia tunnel, both in the large and small subunits, were mutated in an attempt to better evaluate their role in the transport of NH_3. All of the mutants, with the exception of C232G/A251G/A314G were meant to engineer blockages along the path for the migration of ammonia to the second active site in CPS. These residues are fully conserved in CPS from other organisms. The residues for mutagenesis were selected based on their participation in the shuttling of ammonia to the active site for carboxy phosphate formation as determined by the MD simulations. Ser-35 was mutated to a tyrosine in an attempt to position the phenolic side chain across the ammonia tunnel and potentially form hydrogen bonds with Gln-262 and Asp-258. In the MD simulations this mutation nearly blocked the tunnel by forming hydrogen bonds with Gln-262 and Asp-258 across the ammonia tunnel, while the relative distances between the C_α atoms of the residues involved were not significantly changed (shifts < 0.5Å).

The C232V/A251V/A314V mutant in the large subunit was designed to block the ammonia tunnel by introducing a hydrophobic barrier. The valine residues in this mutant enzyme were predicted to come together in the middle of the tunnel through a hydrophobic collapse. This "greasy" plug inside the tunnel would diminish the size of the tunnel diameter. These residues

were also mutated to glycine in an effort to remove any steric hindrance that may have been the cause of the relatively large energy barrier (Figure 3).

Thr-249, which is the residue responsible for forming a hydrogen bond with ammonia after it passes through the turning gate, was mutated to a valine in order to remove this hydrogen bond. Without this interaction in place it may be more difficult for ammonia to enter the water pocket immediately after exiting the turning gate composed of Cys-232, Ala-251, and Ala-314. It was anticipated that this mutant would exhibit a low rate of carbamoyl phosphate synthesis as well as a lower rate for the glutamine-dependent ATPase reaction.

Several other approaches were used to assess the energy barrier created by the C232/A251/A314 triad. Ala-251 and Ala-314 were mutated to cysteine to initiate the formation of an internal disulfide bond with Cys-232. In addition, the A311L and I352F mutations in the ammonia tunnel took advantage of the inward pointing side chains of the alanine and isoleucine residues directly behind the triad. The alanine side chain was mutated to a much larger leucine side chain to create a barrier that would be directly behind the narrowest part of the tunnel, thus inhibiting the passage of ammonia to the active site for carboxy phosphate formation. The isoleucine side chain was mutated to a phenylalanine in a similar attempt to create a larger hydrophobic barrier.

Characterization of Mutants

All of the mutants were analyzed by circular dichroism. The single and triple mutations did not have any effect on the overall structure of the protein (see Supporting Information). The kinetic data in Tables 1 and 2 show that the S35Y mutation did not have a significant effect in blocking the ammonia tunnel. This was most evident from the wild type-like kinetic constants for the glutamine-dependent ATPase reaction. However, this mutation did cause a 10-fold drop in k_{cat} and a 10-fold increase in the K_m for ATP in the bicarbonate-dependent ATPase reaction. The ATP-dependent glutaminase reaction catalyzed by the small subunit remained unaffected by this mutation. The substitution of a tyrosine in place of serine apparently did not promote the formation of a hydrogen bonding network across the tunnel. Since this residue also has a hydroxyl group, but on a larger side chain, it may be that this group can still participate in hydrogen bonding with NH_3 or is unable to slow down the hydrogen bond exchange between ammonia and water clusters in the tunnel.

The C232V/A251V/A314V mutant was unable to synthesize carbamoyl phosphate using glutamine as the nitrogen source. However, the rate of glutamine hydrolysis in the presence of ATP is slightly elevated and significantly increased in the absence of ATP, relative to the wild type enzyme (Table 3). This increase in activity may be due to the larger residues mimicking the movement of the α-helix that expands the gate in the presence of carboxy phosphate. This movement may be part of the signal transduction network between the active sites for carboxy phosphate and glutamine. The formation of carboxy phosphate is decoupled from the hydrolysis of glutamine.[55]

Even though the rate of glutamine hydrolysis was increased no carbamoyl phosphate was synthesized by this mutant. The ability of the triple mutant to utilize ammonia from solvent was comparable to its ability to utilize glutamine. The rate constant for the NH_4^+-dependent ATPase reaction with this mutant was 0.072 ± 0.002 s^{-1} and the K_m was 5.0 ± 0.8 mM. These values are significantly different from the wild type values for the NH_4^+-dpendent ATPase reaction (k_{cat} = 3.9 ± 0.1 s^{-1}, K_m = 130 ± 13 mM [56]), but similar to those measured with this mutant for the Gln-dependent ATPase reaction (Tables 1 and 2). The only partial reaction not affected by this mutation was the ATP synthesis reaction. This result is consistent with a physical blockage created in the tunnel that only affects the transport of ammonia.

The triple glycine mutant was constructed with the intent to lower the energy barrier observed at the C232/A251/A314 triad. However, the kinetic constants for this mutant were not kinetically different from the wild type enzyme. No enhancements in the rate constants for any of the reactions were observed. The mutation itself may have created a larger opening for ammonia to pass through the tunnel, but it was not possible to observe this experimentally, since the transport of ammonia is apparently not rate-limiting.

The single mutants used to study the narrow portion of the tunnel: C251A, A314C, I352F, T249V, and A311L (with the exception of A311L) only slightly interfere with the passage of ammonia through the tunnel. The two cysteine mutants exhibited wild type-like kinetic constants in all of the reactions tested. These data suggest that an internal disulfide bond was not formed. Likewise, the mutant enzymes I352F and T249V possessed wild type-like kinetic constants that suggest that the phenylalanine was not large enough to "plug" the tunnel and that the removal of the hydrogen bond interaction between NH_3 and Thr-249 is insufficient to prevent ammonia from translocating through the tunnel. There was an uncoupling of reactions observed between the glutaminase and carboxy phosphate active sites in the A311L mutant. This is exemplified by the 10-fold decrease in the rate of the glutamine-dependent ATPase reaction. The effectiveness of this single mutation can also be seen in the lowered rate for the carbamoyl phosphate synthesis reaction. These data suggest that A311L may interfere with the passage of ammonia.

Conclusion

The MD simulations reported here provide strong evidence for the existence and function of a sealed molecular tunnel for the transport of ammonia from the site of formation to the site of utilization. Conventional MD simulations for each section of the nearly 60-Å tunnel indicate that the passageway is tightly sealed since leakage of ammonia is never observed. The transfer of ammonia through this tunnel is a rapid process with a free energy barrier of 7.2 kcal/mol at a gate that is formed by the convergence of Cys-232, Ala-251 and Ala-314. The initial injection of the ammonia into the tunnel is favored with a large free energy drop of at least 7 kcal/mol. When ammonia passes the tunnel exit from the small subunit near Thr-37, it enters an area filled with approximately 27 waters, which associate together by forming hydrogen bonds. Tyr-261 from the large subunit splits these water molecules into two clusters. The transfer of the ammonia is favored by a free energy potential from Thr-37 to a gate enclosed by the side chains of Cys-232, Ala-251 and Ala-314. The remaining part of tunnel is enclosed by an α-helix and a β-strand, which form an extremely hydrophobic environment. Most strikingly, the ammonia is desolvated when it passes through the triangular gate. Thr-249 from the β-strand is responsible for the delivery of the ammonia from the gate to the hydrophilic region of the ATP binding site. The side chains of Ile-234 and Leu-310 narrow the path and create a barrier of about 3 kcal/mol before the ammonia reaches the end of the tunnel. These calculations indicate that the rate-determining step for the migration of ammonia is localized to the gate formed by the intersection of C232-A251-A314. A triple mutant, C232V/A251V/A314V, was design to virtually block or impede the migration of ammonia through this narrow passage. The rate of ATP hydrolysis is decreased by a factor of 180 and the synthesis of carbamoyl phosphate is not observed. However, the functional properties at the site of carbamoyl phosphate synthesis (as measured by the synthesis of ATP from carbamoyl phosphate and ADP) are not damaged. Furthermore, based on PMF calculations for different ligands binding to the site for carbamate formation, it appears that the synthesis of carboxy phosphate lowers the barrier at the narrowest gate by about 2 kcal/mol. Therefore, the formation of the carboxy phosphate intermediate may enhance the transport of ammonia through the tunnel and serve as an allosteric regulator.

Supplementary Material

Refer to Web version on PubMed Central for supplementary material.

ACKNOWLEDGMENT

This work was supported in part by the Robert A. Welch Foundation (A-840 to FMR and A-1628 to YQG) and the NIH (DK 030343 to FMR). The supercomputer facilities at Texas A&M University were supported by the NSF (NSF-DMS 0216275). YQG is a 2006 Searle Scholar.

REFERENCES

1. Anderson PM. Biochemistry 1977;16:587–593. [PubMed: 189806]
2. Anderson PM, Meister A. Biochemistry 1966;5:3164–3169. [PubMed: 5339550]
3. Pierard A, Wiame JM. Biochem. Biophys. Res. Commun 1964;15:76–81. [PubMed: 5319709]
4. Anderson PM. Biochemistry 1977;16:587–93. [PubMed: 189806]
5. Raushel FM, Anderson PM, Villafranca JJ. Biochemistry 1978;17:5587–91. [PubMed: 215204]
6. Raushel FM, Villafranca JJ. Biochemistry 1979;18:3424–9. [PubMed: 223631]
7. Mergeay M, Gigot D, Beckmann J, Glansdor N, Pierard A. Mol. Gen. Genet 1974;133:299–316. [PubMed: 4373646]
8. Piette J, Nyunoya H, Lusty CJ, Cunin R, Weyens G, Crabeel M, Charlier D, Glansdorff N, Pierard A. Proc. Natl. Acad. Sci. U. S. A 1984;81:4134–4138. [PubMed: 6330744]
9. Miran SG, Chang SH, Raushel FM. Biochemistry 1991;30:7901–7. [PubMed: 1868065]
10. Thoden JB, Raushel FM, Benning MM, Rayment I, Holden HM. Acta Crystallogr D Biol Crystallogr 1999;55:8–24. [PubMed: 10089390]
11. Thoden JB, Holden HM, Wesenberg G, Raushel FM, Rayment I. Biochemistry 1997;36:6305–6316. [PubMed: 9174345]
12. Krahn JM, Kim JH, Burns MR, Parry RJ, Zalkin H, Smith JL. Biochemistry 1997;36:11061–11068. [PubMed: 9333323]
13. Larsen TM, Boehlein SK, Schuster SM, Richards NGJ, Thoden JB, Holden HM, Rayment I. Biochemistry 1999;38:16146–16157. [PubMed: 10587437]
14. van den Heuvel RHH, Ferrari D, Bossi RT, Ravasio S, Curti B, Vanoni MA, Florencio FJ, Mattevi A. J. Biol. Chem 2002;277:24579–24583. [PubMed: 11967268]
15. Douangamath A, Walker M, Beismann-Driemeyer S, Vega-Fernandez MC, Sterner R, Wilmanns M. Structure 2002;10:185–193. [PubMed: 11839304]
16. Mouilleron S, Badet-Denisot MA, Golinelli-Pimpaneau B. J. Biol. Chem 2006;281:4404–4412. [PubMed: 16339762]
17. Teplyakov A, Obmolova G, Badet B, Badet-Denisot MA. J. Mol. Biol 2001;313:1093–1102. [PubMed: 11700065]
18. Schmitt E, Panvert M, Blanquet S, Mechulam Y. Structure 2005;13:1421–1433. [PubMed: 16216574]
19. LaRonde-LeBlanc N, Resto M, Gerratana B. Nat. Struct. Mol. Biol 2009;16:421–429. [PubMed: 19270703]
20. Wojcik M, Seidle HF, Bieganowski P, Brenner C. J. Biol. Chem 2006;281:33395–33402. [PubMed: 16954203]
21. Raushel FM, Thoden JB, Holden HM. Acc. Chem. Res 2003;36:539–548. [PubMed: 12859215]
22. Weeks A, Lund L, Raushel FM. Curr. Opin. Chem. Biol 2006;10:465–472. [PubMed: 16931112]
23. Mullins LS, Raushel FM. J. Am. Chem. Soc 1999;121:3803–3804.
24. Yang HY, Xu YC, Zhu WL, Chen KX, Jiang HL. Biophys. J 2007;92:877–885. [PubMed: 17098799]
25. Fan Y, Lund L, Yang LJ, Raushel FM, Gao YQ. Biochemistry 2008;47:2935–2944. [PubMed: 18220365]
26. Thoden JB, Huang XY, Raushel FM, Holden HM. Biochemistry 1999;38:16158–16166. [PubMed: 10587438]

27. Schwede T, Kopp J, Guex N, Peitsch MC. Nucleic Acids Res 2003;31:3381–3385. [PubMed: 12824332]
28. Kopp J, Schwede T. Nucleic Acids Res 2004;32:D230–D234. [PubMed: 14681401]
29. Arnold K, Bordoli L, Kopp J, Schwede T. Bioinformatics 2006;22:195–201. [PubMed: 16301204]
30. Singh UC, Kollman PA. J. Comput. Chem 1984;5:129–145.
31. Besler BH, Merz KM, Kollman PA. J. Comput. Chem 1990;11:431–439.
32. Becke AD. Phys. Rev. A: At. Mol. Opt. Phys 1988;38:3098–3100.
33. Lee CT, Yang WT, Parr RG. Phys. Rev. B: Condens. Matter 1988;37:785–789. [PubMed: 9944570]
34. Becke AD. J. Chem. Phys 1993;98:1372–1377.
35. Kendall RA, Dunning TH, Harrison RJ. J. Chem. Phys 1992;96:6796–6806.
36. Cances E, Mennucci B, Tomasi J. J. Chem. Phys 1997;107:3032–3041.
37. Cossi M, Barone V, Mennucci B, Tomasi J. Chem. Phys. Lett 1998;286:253–260.
38. Mennucci B, Tomasi J. J. Chem. Phys 1997;106:5151–5158.
39. Jorgensen WL, Chandrasekhar J, Madura JD, Impey RW, Klein ML. J. Chem. Phys 1983;79:926–935.
40. Case, DA., et al. AMBER 9. University of California; San Francisco: 2006.
41. Case, DA., et al. AMBER 8. University of California; San Francisco: 2004.
42. Wang JM, Cieplak P, Kollman PA. J. Comput. Chem 2000;21:1049–1074.
43. Wang JM, Wolf RM, Caldwell JW, Kollman PA, Case DA. J. Comput. Chem 2004;25:1157–1174. [PubMed: 15116359]
44. Meagher KL, Redman LT, Carlson HA. J. Comput. Chem 2003;24:1016–1025. [PubMed: 12759902]
45. Bradbrook GM, Gleichmann T, Harrop SJ, Habash J, Raftery J, Kalb J, Yariv J, Hillier IH, Helliwell JR. J. Chem. Soc., Faraday Trans 1998;94:1603–1611.
46. Vangunsteren WF, Berendsen HJC. Mol. Phys 1977;34:1311–1327.
47. Darden T, York D, Pedersen L. J. Chem. Phys 1993;98:10089–10092.
48. Essmann U, Perera L, Berkowitz ML, Darden T, Lee H, Pedersen LG. J. Chem. Phys 1995;103:8577–8593.
49. Kottalam J, Case DA. J. Am. Chem. Soc 1988;110:7690–7697.
50. Kumar S, Bouzida D, Swendsen RH, Kollman PA, Rosenberg JM. J. Comput. Chem 1992;13:1011–1021.
51. Kumar S, Rosenberg JM, Bouzida D, Swendsen RH, Kollman PA. J. Comput. Chem 1995;16:1339–1350.
52. Roux B. Comput. Phys. Commun 1995;91:275–282.
53. Vallequ, J. P. a. T., G. M. Statistical Mechanics, Part A, Equilibiurm Techniques. Vol. 5. Plenum Press; New York: 1977.
54. Mareya SM, Raushel FM. Biochemistry 1994;33:2945–2950. [PubMed: 8130208]
55. Miles BW, Raushel FM. Biochemistry 2000;39:5051–5056. [PubMed: 10819970]
56. Kim J, Raushel FM. Biochemistry 2004;43:5334–5340. [PubMed: 15122899]
57. Stapleton MA, JavidMajd F, Harmon MF, Hanks BA, Grahmann JL, Mullins LS, Raushel FM. Biochemistry 1996;35:14352–14361. [PubMed: 8916922]
58. Kramers HA. Phys 1940;7:284–304.
59. Berne BJ, Borkovec M, Straub JE. J. Phys. Chem 1988;92:3711–3725.
60. Socci ND, Onuchic JN, Wolynes PG. J. Chem. Phys 1996;104:5860–5868.

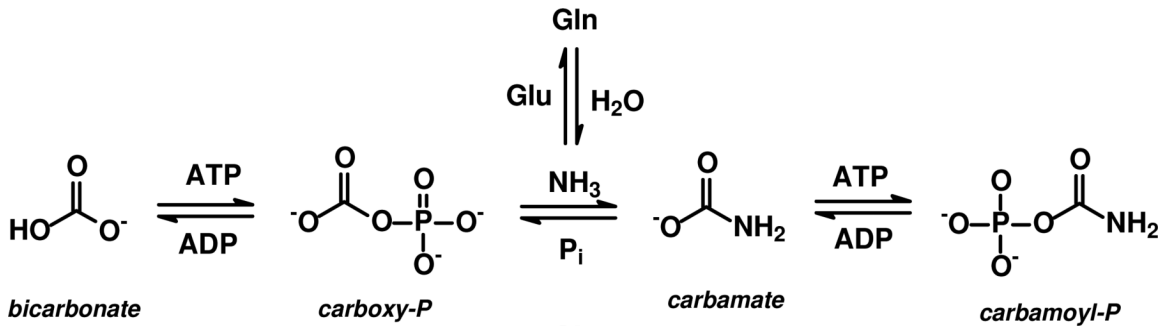

Scheme 1.

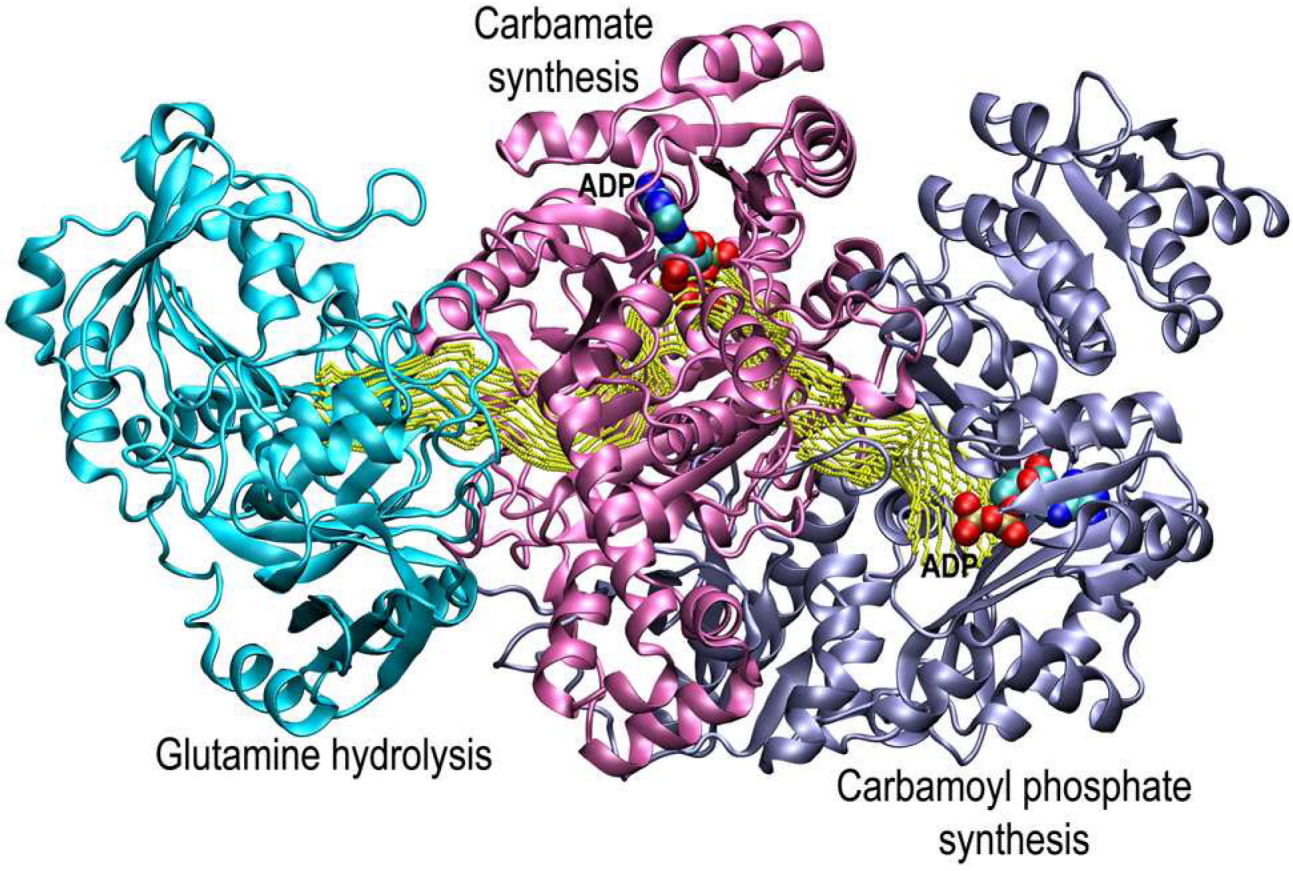

Figure 1.
The structure of carbamoyl phosphate synthetase. The small subunit that contains the active site for the hydrolysis of glutamine is shown in green. The N-terminal domain of the large subunit that contains the active site for the synthesis of carboxy phosphate and carbamate is shown in red. The C-terminal domain of the large subunit that contains the active site for the synthesis of carbamoyl phosphate is shown in blue. The two molecular tunnels for the translocation of ammonia and carbamate are shown in yellow dotted lines. The image was constructed from PDB file: 1C3O.

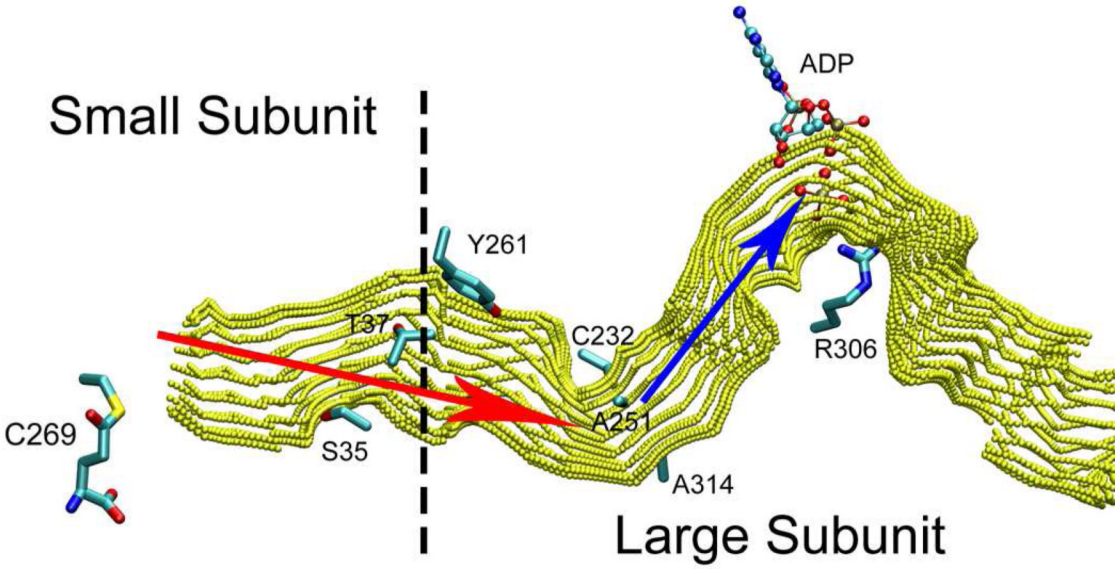

Figure 2.

The molecular tunnel for the transport of ammonia from the site of the glutamine hydrolysis to the site of the carbamate formation. The entire tunnel is separated into two parts, illustrated by the two arrows that are separated by the triangular gate formed by Cys-232, Ala-251 and Ala-314. The black dashed line divides the tunnel at the interface of the small and large subunits. Ser-35 and Thr-37 are the connecting points. Cys-269 is at the beginning of the ammonia tunnel while ADP, P_i and Arg-306 are at the end.

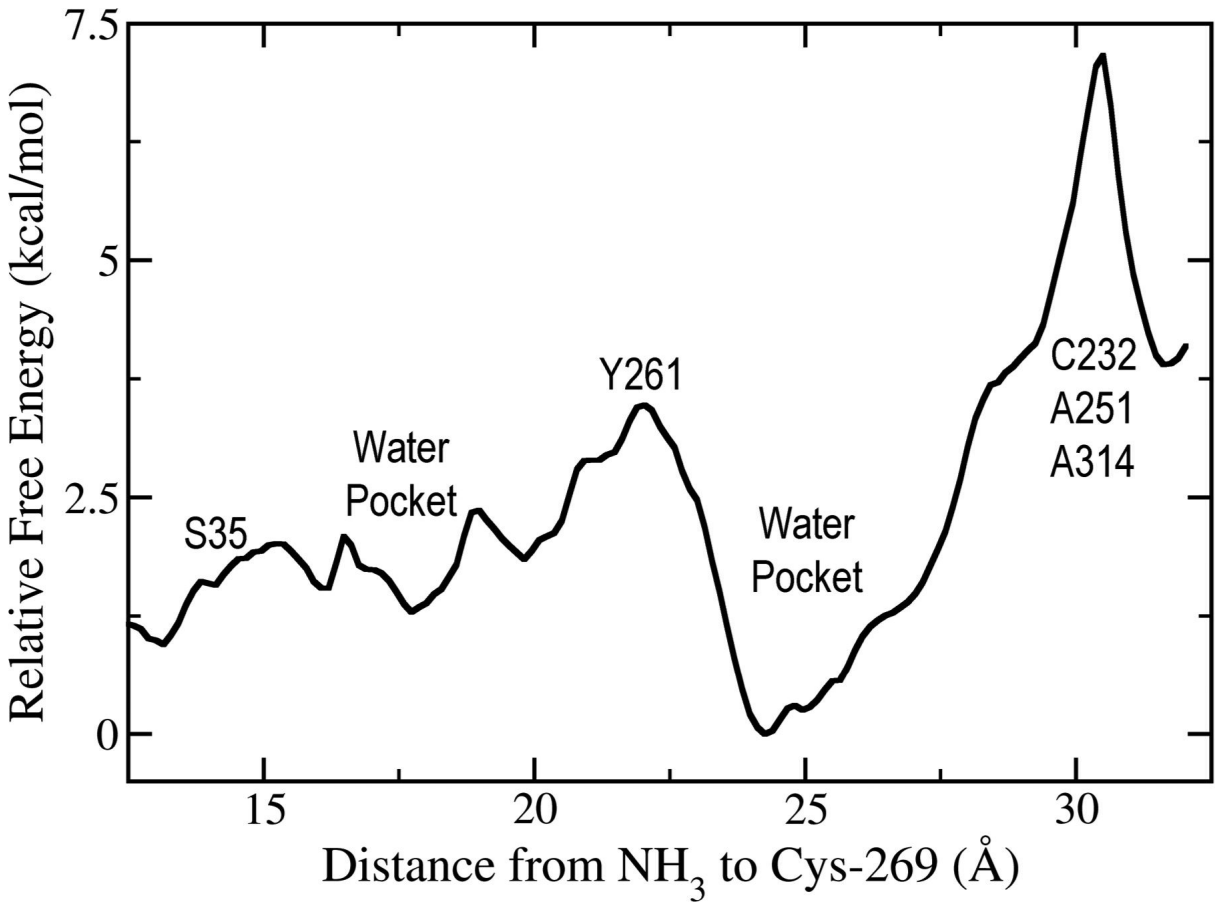

Figure 3.
Potentials of mean force from Thr-37 in the small subunit to the narrow turn surrounded by Cys-232, Ala-251 and Ala-314. The reaction coordinate is defined as the distance from the nitrogen atom in the ammonia to the carbonyl carbon of the thioester intermediate in Cys-269.

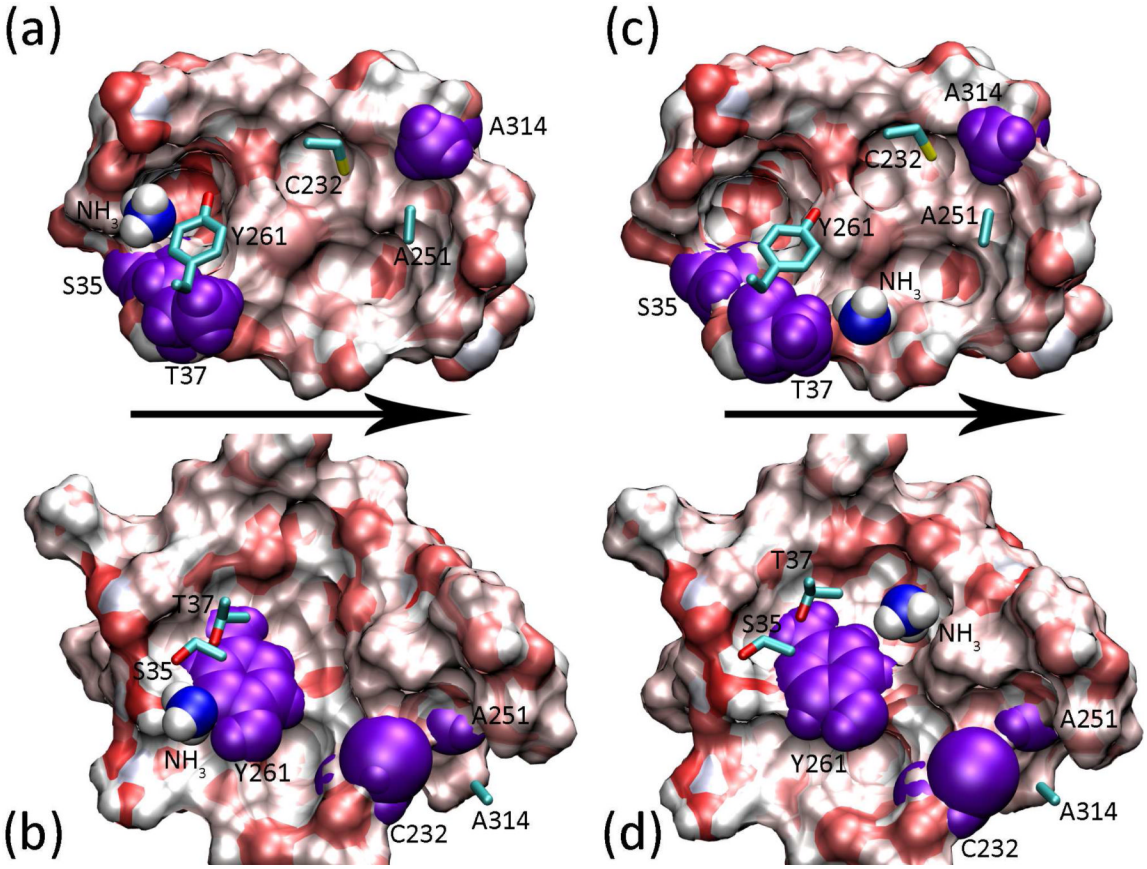

Figure 4.

The solvated ammonia (waters are not shown) in the water pockets at the interface between the small and large subunits: (a) and (b) are the two halves of the ammonia tunnel when ammonia is in the first pocket between Thr-37 and Tyr-261; (c) and (d) when ammonia is in the second pocket between Tyr-261 and the turning gate surrounded by Cys-232, Ala-251 and Ala-314. The surface model is used to depict the impenetrable and well-shaped pocket wall. The arrows stand for the direction of the ammonia transport.

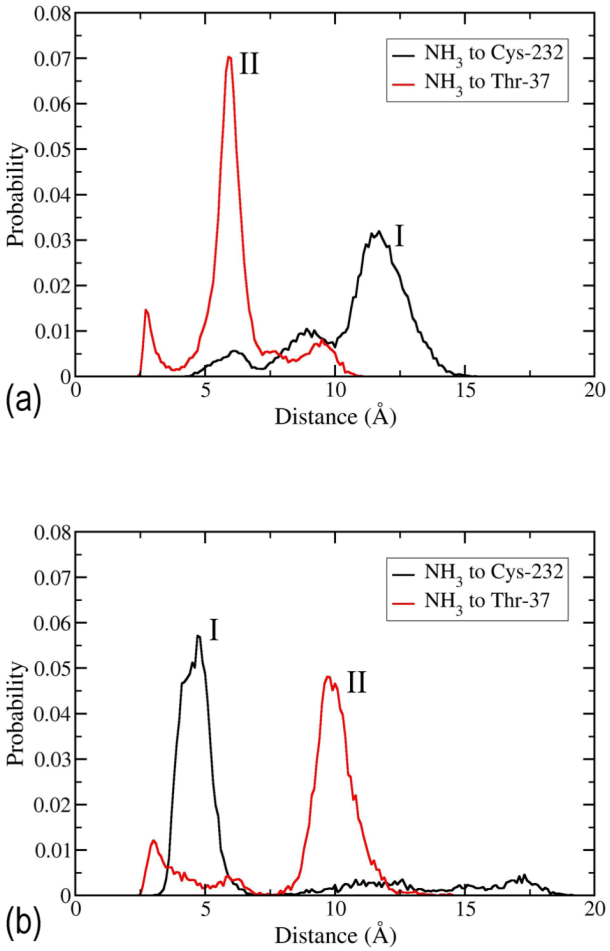

Figure 5.

Probability distribution of the distances from the nitrogen atom in ammonia to: (a) the Cβ in Cys-232 (black); (b) the oxygen atom of the side chain hydroxyl in Thr-37 (red). The probability distributions obtained from the 5-ns trajectory started with the ammonia positioned between Thr-37 and Tyr-261 are labeled by (I) while the ones from the 16-ns trajectory started with the ammonia positioned between Tyr-261 and Cys-232 are labeled by (II).

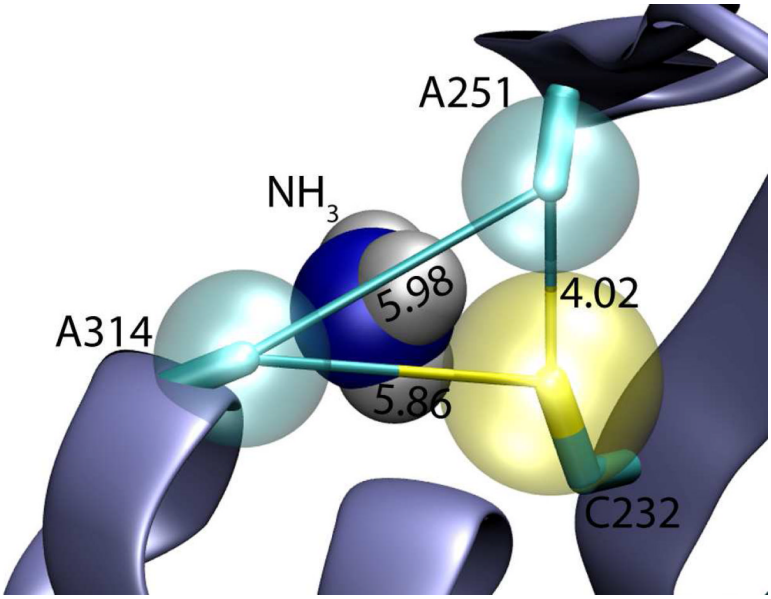

Figure 6.
The triangular gate surrounded by Cys-232, Ala-251 and Ala-314 leading to the site of carbamate formation. The van der Waals spheres for the sulfur atom of Cys-232 and C_α atoms of Ala-251 and Ala-314 are shown in transparency. The distances are in Å.

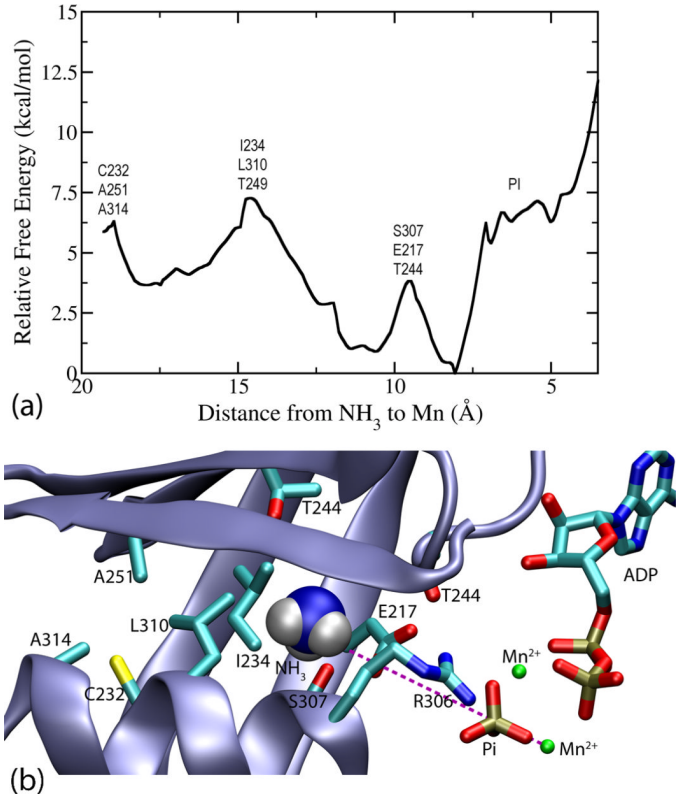

Figure 7.

(a) Potentials of mean force (PMF) *vs*. the distance from the nitrogen atom in ammonia to one of the manganese ions at the site of carbamate formation (see **Figure 7b**); (b) the tunnel structure from the gate surrounded by Cys-232, Ala-251 and Ala-314 to the site of carbamate formation. The reaction coordinate is shown in magenta as a dotted line. The three barriers shown in **Figure 7a** correspond to the relatively narrow parts formed by the triads, C232-A251-A314, I234-T249-L310 and E217-T244-S307, respectively. In **Figure 7b**, the ammonia is positioned between the second and third triads.

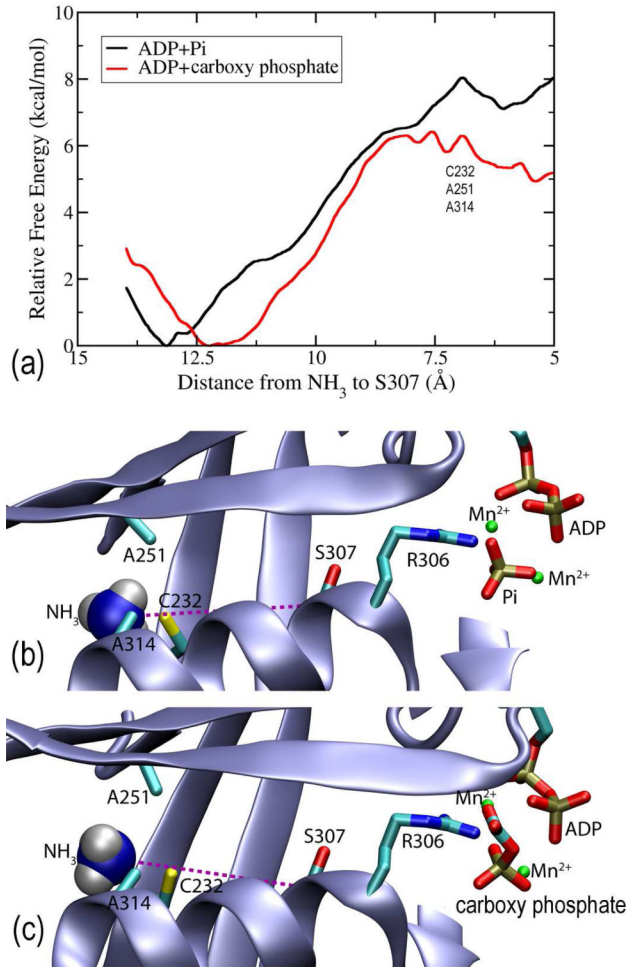

Figure 8.

(a) Potentials of mean force (PMF) *vs* the distance from the nitrogen atom in ammonia to the C_α of Ser-307 in the large subunit; (b) the reaction coordinate (dotted line in magenta) for the umbrella sampling and the structure with bound P_i; (c) the reaction coordinate (dotted line in magenta) for the umbrella sampling and the structure of the bound carboxy phosphate intermediate.

Table 1

Kinetic characterization of the wild type and mutant forms of CPS[a].

	Gln-dependent ATPase		HCO_3^--dependent ATPase[b]		ATP-dependent Glutaminase	
Enzyme	k_{cat} (s^{-1})	K_m (mM ATP)	k_{cat} (s^{-1})	K_m (mM ATP)	k_{cat} (s^{-1})	K_m (mM Gln)
WT	3.6 ± 0.1	0.24 ± 0.04	0.17 ± 0.01	0.051 ± 0.008	2.2 ± 0.1	0.15 ± 0.01
S35Y	3.7 ± 0.1	0.43 ± 0.04	0.079 ± 0.002	0.18 ± 0.03	2.7 ± 0.1	0.27 ± 0.05
C232V/A251V/A314V	0.020 ± 0.001	1.6 ± 0.3	0.011 ± 0.002	2.9 ± 0.9	4.5 ± 0.1	0.19 ± 0.03
C232G/A251G/A314G	2.0 ± 0.1	0.06 ± 0.01	0.26 ± 0.01	0.13 ± 0.01	1.5 ± 0.1	0.15 ± 0.01
A251C	2.4 ± 0.1	0.07 ± 0.01	0.30 ± 0.01	0.036 ± 0.007	1.6 ± 0.1	0.25 ± 0.05
A314C	2.3 ± 0.1	0.08 ± 0.01	0.35 ± 0.01	0.014 ± 0.002	0.93 ± 0.03	0.18 ± 0.02
A311L	0.78 ± 0.01	0.15 ± 0.02	0.18 ± 0.01	0.13 ± 0.002	1.6 ± 0.1	0.45 ± 0.06
I352F	3.4 ± 0.2	0.32 ± 0.09	0.15 ± 0.01	0.08 ± 0.01	1.1 ± 0.1	0.19 ± 0.02
T249V	1.8 ± 0.1	0.07 ± 0.01	0.45 ± 0.01	0.035 ± 0.004	1.4 ± 0.1	0.06 ± 0.01

[a] All mutations with the exception of S35Y were made in the large subunit.

[b] HCO_3^--dependent ATPase activity was measured in the absence of glutamine.

J Am Chem Soc. Author manuscript; available in PMC 2010 July 29.

Table 2

Kinetic characterization of ATP and carbamoyl phosphate (CP) synthesis activities.

	ATP-Synthesis[a]		CP Synthesis	ATP:CP
enzyme	k_{cat} (s^{-1})	K_m (mM ADP)	k_{cat} (s^{-1})	
WT	0.13 ± 0.01	0.13 ± 0.03	1.9 ± 0.01	1.9
S35Y	0.17 ± 0.01	0.14 ± 0.02	1.0 ± 0.01	3.7
C232V/A251V/A314V	0.28 ± 0.01	0.12 ± 0.02	ND	ND
C232G/A251G/A314G	0.09 ± 0.01	0.054 ± 0.006	0.89 ± 0.01	2.2
A251C	0.10 ± 0.01	0.044 ± 0.009	0.81 ± 0.01	3.0
A314C	0.10 ± 0.05	0.045 ± 0.006	0.73 ± 0.02	3.1
A311L	0.10 ± 0.01	0.15 ± 0.02	0.29 ± 0.01	2.7
I352F	0.24 ± 0.01	0.15 ± 0.02	1.08 ± 0.01	3.1
T249V	0.22 ± 0.01	0.056 ± 0.005	0.90 ± 0.01	2.0

[a] From ADP and carbamoyl phosphate.

Table 3

ATP-free glutaminase activity

Enzyme	k_{cat} (s^{-1})	K_m (mM Gln)
Wild Type	0.072 ± 0.006	0.32 ± 0.08
C232V/A251V/A314V	1.5 ± 0.19	0.50 ± 0.16